

for *Astrophysical Journal*, November 9, 2018

Quenching of Carbon Monoxide and Methane in the Atmospheres of Cool Brown Dwarfs and Hot Jupiters

Channon Visscher¹, and Julianne I. Moses²

¹*Lunar and Planetary Institute, USRA, 3600 Bay Area Blvd, Houston, TX 77058*

²*Space Science Institute, 4750 Walnut St, Suite 205, Boulder, CO 80301*

visscher@lpi.usra.edu, jmoses@spacescience.org

ABSTRACT

We explore $\text{CO} \rightleftharpoons \text{CH}_4$ quench kinetics in the atmospheres of substellar objects using updated time-scale arguments, as suggested by a thermochemical kinetics and diffusion model that transitions from the thermochemical-equilibrium regime in the deep atmosphere to a quench-chemical regime at higher altitudes. More specifically, we examine CO quench chemistry on the T dwarf Gliese 229B and CH_4 quench chemistry on the hot-Jupiter HD 189733b. We describe a method for correctly calculating reverse rate coefficients for chemical reactions, discuss the predominant pathways for $\text{CO} \rightleftharpoons \text{CH}_4$ interconversion as indicated by the model, and demonstrate that a simple time-scale approach can be used to accurately describe the behavior of quenched species when updated reaction kinetics and mixing-length-scale assumptions are used. Proper treatment of quench kinetics has important implications for estimates of molecular abundances and/or vertical mixing rates in the atmospheres of substellar objects. Our model results indicate significantly higher K_{zz} values than previously estimated near the CO quench level on Gliese 229B, whereas current model-data comparisons using CH_4 permit a wide range of K_{zz} values on HD 189733b. We also use updated reaction kinetics to revise previous estimates of the Jovian water abundance, based upon the observed abundance and chemical behavior of carbon monoxide. The CO chemical/observational constraint, along with *Galileo* entry probe data, suggests a water abundance of approximately $0.51 - 2.6 \times$ solar (for a solar value of $\text{H}_2\text{O}/\text{H}_2 = 9.61 \times 10^{-4}$) in Jupiter's troposphere, assuming vertical mixing from the deep atmosphere is the only source of tropospheric CO.

Subject headings: astrochemistry — planets and satellites: individual (Jupiter) — stars: low-mass, brown dwarfs — stars: individual (Gliese 229, HD 189733) — stars: planetary systems

arXiv:1106.3525v1 [astro-ph.EP] 17 Jun 2011

1. Introduction

In general, thermochemical equilibrium governs the composition of the deep atmospheres of giant planets and brown dwarfs because they are warm enough for chemical reactions to readily overcome energy barriers to reaction kinetics. However, disequilibrium processes in substellar atmospheres are well known. In addition to photochemistry driven by ultraviolet irradiation, atmospheric mixing is one of the dominant mechanisms that drives the chemical composition out of equilibrium. In this scenario, rapid vertical mixing may transport a parcel of gas to higher, cooler altitudes before its chemical constituents have had sufficient time to attain equilibrium via reaction chemistry — a phenomenon that has been proposed to explain the overabundance of various “disequilibrium” species in the atmospheres of Jupiter, Saturn, Uranus, and Neptune (e.g., Prinn & Owen 1976; Prinn & Barshay 1977; Barshay & Lewis 1978; Fegley & Lewis 1979; Prinn & Olaguer 1981; Prinn et al. 1984; Lewis & Fegley 1984; Fegley & Prinn 1985, 1986, 1988; Fegley et al. 1991; Fegley & Lodders 1994; Lodders & Fegley 1994, 2002; Bézard et al. 2002; Taylor et al. 2004; Visscher & Fegley 2005; Fouchet et al. 2009; Visscher et al. 2010; Moses et al. 2010), brown dwarfs (e.g., Fegley & Lodders 1996; Noll et al. 1997; Griffith & Yelle 1999; Griffith 2000; Saumon et al. 2000; Lodders & Fegley 2002; Golimowski et al. 2004; Saumon et al. 2006, 2007; Visscher et al. 2006; Leggett et al. 2007; Hubeny & Burrows 2007; Geballe et al. 2009; King et al. 2010; Yamamura et al. 2010), and extrasolar giant planets (e.g., Cooper & Showman 2006; Fortney et al. 2006b; Burrows et al. 2008; Line et al. 2010; Madhusudhan & Seager 2011; Stevenson et al. 2010; Moses et al. 2011).

Prinn & Barshay (1977) first developed an analytical model to explain the observed overabundance of CO in Jupiter’s troposphere due to strong vertical mixing. In this approach, a time scale for convective mixing (τ_{mix}), based upon an estimated mixing length scale and vertical mixing rate, is compared to a time scale for chemical kinetics (τ_{chem}), based upon an assumption about which chemical pathways will be important for interconversion between atmospheric constituents. At high temperatures in the deep atmosphere, thermochemical equilibrium is maintained because reaction kinetics operate faster than convective mixing (*i.e.*, $\tau_{chem} < \tau_{mix}$). However, departures from equilibrium can occur at colder, higher altitudes when convective mixing begins to dominate over reaction kinetics (*i.e.*, when $\tau_{chem} > \tau_{mix}$), and the abundance of a molecular constituent may become “quenched” at a value representative of the quench level (defined by $\tau_{chem} = \tau_{mix}$). This level is different for each species (Fegley & Prinn 1985) and, in principle, *every* species that is subject to reaction chemistry and atmospheric transport will quench if the appropriate time scale for reaction kinetics becomes longer than the time scale for convective mixing (e.g., see Fig. 6 in Visscher et al. 2010). Here we investigate the chemical interconversion between CO and CH₄, which becomes quenched when $\tau_{chem}(\text{CO} \rightleftharpoons \text{CH}_4) > \tau_{mix}$ in a substellar at-

mosphere. Whether either species is considered a “disequilibrium” species depends upon its quench abundance relative to its expected equilibrium abundance at higher altitudes. For example, CO is present as a disequilibrium species on objects where CH₄ is the dominant carbon-bearing gas, including Jupiter and T dwarfs (such as Gliese 229B), whereas CH₄ is present as a disequilibrium species on objects where CO is the dominant carbon-bearing gas, including L dwarfs and hot Jupiters (such as HD 189733b and HD 209458b).

Although the general approach of Prinn & Barshay (1977) is robust, uncertainties in identifying the rate-limiting step for CO \rightleftharpoons CH₄ interconversion, errors in the treatment of reaction kinetics, and incorrect assumptions about the mixing length scale are found throughout the astrophysical literature for substellar objects. As we discuss below, these issues may lead to incorrect conclusions regarding quench abundances for disequilibrium species and/or incorrect estimates of atmospheric mixing rates that are constrained by the disequilibrium chemistry. In order to circumvent some of the uncertainties involved with traditional time-scale modeling approaches, we recently developed a one-dimensional photochemistry, thermochemistry, and transport model for the atmosphere of Jupiter (Visscher et al. 2010; Moses et al. 2010) and extrasolar giant planets (Moses et al. 2011). This approach allows us to accurately model the abundance of constituents in the transition region between the thermochemical regime in the deep troposphere (where equilibrium is maintained via rapid reaction kinetics) and the quenched regime in the upper troposphere (where rapid atmospheric transport and slow reaction kinetics drive constituents out of equilibrium). Our models show that the reactions previously used to predict quenching of CO and CH₄ on giant planets and brown dwarfs may not be the rate-limiting steps in the quenching process. Because of this result and previously described problems with mixing length scale assumptions (Smith 1998), the time-scale arguments require several updates, which are presented here. Due to the overall uncertainties in the CO \rightleftharpoons CH₄ kinetic pathways, the rate-limiting reactions identified by our thermochemical kinetics and transport model may change with advances in our understanding of C-H-O kinetics at high temperatures under reducing conditions. As such, we also outline procedures that can be used to help derive τ_{chem} for any other potential rate-limiting reaction in the CO \rightleftharpoons CH₄ interconversion mechanism, specifically for cases in which existing rate coefficients need to be reversed. To illustrate the use of these time-scale arguments, transport-induced quenching of CO in the atmosphere of the T dwarf Gliese 229B and the quenching of CH₄ in the atmosphere of the hot-Jupiter HD 189733b become our specific examples to be discussed in detail.

Our primary objectives are to 1) describe a method for correctly reversing chemical reactions using the principle of microscopic reversibility, 2) identify the dominant chemical pathways for the quenching of CO and CH₄ on Gliese 229B and HD 189733b, respectively, as determined from the results of the kinetics-and-transport model, and 3) describe revisions

to simple time-scale arguments that can be used to more accurately predict the quenched abundances of either CO or CH₄ in substellar objects. We also revise our estimate of the water abundance in Jupiter’s deep troposphere (Visscher et al. 2010) based upon updates to the CO → CH₄ kinetic scheme. Throughout the following, we focus on thermochemistry and mixing only, without photochemistry, in order to specifically examine the effect of atmospheric transport on the abundances of key atmospheric constituents.

2. Chemical Model

2.1. Numerical Approach

Our chemical model is based upon a thermochemical kinetics and diffusion model developed for Jupiter (Visscher et al. 2010; Moses et al. 2010) and for the hot-Jupiter exoplanets HD 189733b and HD 209458b (Moses et al. 2011). This one-dimensional (1-D) model, which uses the Caltech/JPL KINETICS code (Allen et al. 1981), is described more completely in the above citations; here, we briefly discuss the salient points. The code uses finite-difference techniques to solve the continuity equations controlling the vertical distribution of neutral carbon-, oxygen-, and nitrogen-bearing constituents. Because 1-D models cannot capture the complex three-dimensional transport processes that result from convection, atmospheric waves, and eddies of all sizes, all such vertical mixing processes are typically approximated in 1-D models as “eddy diffusion” parameterized by the eddy diffusion coefficient K_{zz} . Free-convection and mixing-length theories (Stone 1976; Flasar & Gierasch 1977) help constrain the magnitude of K_{zz} in the deep atmospheres of giant planets and brown dwarfs; however, the constraints are loose, and we consider the K_{zz} profile to be a free parameter in our models. Using mixing-length theory and previous estimates of K_{zz} (e.g., Griffith et al. 1998; Griffith & Yelle 1999; Cooper & Showman 2006; Showman et al. 2009; Lewis et al. 2010; Youdin & Mitchell 2010) as a guide, we examine the sensitivity of our results to variations in K_{zz} values ranging from 10^3 to 10^9 cm² s⁻¹ on Gliese 229B and from 10^7 to 10^{11} cm² s⁻¹ on HD 189733b. The Gliese 229B results described here are new, and a full description of the model results will be presented in a later publication; further details of the HD 189733b model, along with comparisons to other exoplanet chemical models (e.g., Liang et al. 2003, 2004; Zahnle et al. 2009b,a; Line et al. 2010) can be found in Moses et al. (2011).

The pressure-temperature profiles adopted for our models are shown in Figure 1. The profile for Gliese 229B is taken from Model B of Saumon et al. (2000). The profiles for HD 189733b are from Moses et al. (2011) and represent dayside-average and terminator-average thermal structures based upon the 3-D GCM simulations of Showman et al. (2009). These profiles are chosen for their relevance to atmospheric conditions at secondary eclipse and

primary transit, respectively, and include extensions to low pressures using the thermospheric models of García Muñoz (2007) and extensions to high pressures using the 1D models of Fortney et al. (2006a). We adopt protosolar elemental abundances from Lodders et al. (2009), with an assumed $0.5\times$ protosolar composition ($[\text{Fe}/\text{H}] = -0.3$) for Gliese 229B based upon Model B in Saumon et al. (2000), and an assumed $1\times$ protosolar composition ($[\text{Fe}/\text{H}] = 0$) for HD 189733b. For both objects, we assume uniform metallicity for all elements (e.g., solar C/O ratio) and consider the removal of 20% of oxygen by reaction with rock-forming elements in the deep atmosphere (e.g., note silicate condensation curves in Fig. 1; see Lodders 2004; Visscher & Fegley 2005). Thermochemical equilibrium calculations are used to determine the initial atmospheric composition in the absence of transport, as is described in Visscher et al. (2010) and Moses et al. (2010).

2.2. Reaction Kinetics

The reaction list in our thermochemical kinetics and transport model is similar to that described in Visscher et al. (2010) and Moses et al. (2010, 2011). All of the chemical reactions in the model are reversed using the principle of microscopic reversibility. As an aid to other investigators, we discuss this approach in detail to show how reverse rate coefficients are correctly calculated, particularly for reactions with an unequal number of reactants and products. For example, if we consider a balanced, elementary, gas-phase chemical reaction,



there are a molecules of species A, b molecules of species B, and so on, and the expression for the equilibrium constant K_{eq} of the reaction can be written as

$$K_{eq} = \frac{[\text{C}]^c[\text{D}]^d}{[\text{A}]^a[\text{B}]^b}, \quad (2)$$

where $[i]$ is the number density (molecules cm^{-3}) of each species i . The rates (ν) of the forward reaction and reverse reaction are given by

$$\nu_f = k_f[\text{A}]^a[\text{B}]^b \quad (3)$$

$$\nu_r = k_r[\text{C}]^c[\text{D}]^d \quad (4)$$

where k_f and k_r are the kinetic rate coefficients for the forward and reverse reactions, respectively. When the system is operating at equilibrium, the forward reaction rate is equal to the reverse reaction rate:

$$k_f[\text{A}]^a[\text{B}]^b = k_r[\text{C}]^c[\text{D}]^d \quad (5)$$

which is an expression of the principle of microscopic reversibility. Substitution into the equilibrium constant expression (2) gives an equation often found in textbooks,

$$K_{eq} = \frac{k_f}{k_r}, \quad (6)$$

that can be used to determine reverse reaction rate coefficients. However, it is important to note that thermodynamic tabulations containing equilibrium constants (K) are generally calculated assuming units of pressure (e.g., 1-bar constant-pressure reference state, Chase 1998), whereas reaction rate coefficients (k) are generally reported in units of number density. For reactions containing different numbers of reactants and products, omission of the appropriate pressure-correction terms in equation (6) will result in incorrect rate coefficients for the reverse reaction.

For example, several authors consider $\text{H} + \text{H}_2\text{CO} + \text{M} \rightarrow \text{CH}_3\text{O} + \text{M}$ as the rate-limiting step for $\text{CO} \rightarrow \text{CH}_4$ conversion in substellar atmospheres (Yung et al. 1988; Griffith & Yelle 1999; Bézard et al. 2002; Cooper & Showman 2006; Line et al. 2010), where M represents any third body. The rate coefficient for this termolecular reaction has not been measured experimentally, but it can be calculated from the rate coefficient of the reverse reaction $\text{CH}_3\text{O} + \text{M} \rightarrow \text{H} + \text{H}_2\text{CO} + \text{M}$ investigated by Page et al. (1989). As pointed out by Bézard et al. (2002), the pressure-correction term was omitted by Griffith & Yelle (1999) in their reversal, and therefore Griffith & Yelle (1999) have adopted an incorrect rate coefficient in their treatment of CO quench kinetics on Gliese 229B. Line et al. (2010) make a similar error in their treatment of quench kinetics on HD 189733b and derive a two-body rate coefficient (which was subsequently adopted by Madhusudhan & Seager 2011, for GJ 436b) for the three-body reaction $\text{H} + \text{H}_2\text{CO} + \text{M}$. However, because Line et al. (2010) consider a quench level that is near 1 bar, their omission of the pressure-correction term is mostly offset by their omission of the $[\text{M}]$ term when calculating the rate of $\text{H} + \text{H}_2\text{CO} + \text{M}$. Nevertheless, such errors result in inaccurate reaction-rate estimates and may therefore result in incorrect conclusions regarding quench abundances and the strength atmospheric mixing on substellar objects (e.g., Griffith & Yelle 1999; Line et al. 2010; Madhusudhan & Seager 2011), particularly for cases in which the chemical behavior of an observed quenched species is used to constrain the value of the eddy diffusion coefficient.

In order to correctly reverse reactions with different numbers of products and reactants, we derive the appropriate pressure-correction term for equation (6). The equilibrium constant expression for reaction (1) in terms of pressure is written as

$$K_P = e^{-\Delta_r G^\circ / RT} = \frac{P_C^c P_D^d}{P_A^a P_B^b} \quad (7)$$

where R is the gas constant, P_i is the partial pressure (in bars) of each species i , and $\Delta_r G^\circ$

is the Gibbs free energy change for the reaction (J mol^{-1}) at the standard-state pressure (e.g., $P^\circ = 1$ bar; Chase 1998), calculated from the Gibbs free energy of formation of the products and reactants:

$$\Delta_r G^\circ = \Delta_f G^\circ(\text{products}) - \Delta_f G^\circ(\text{reactants}). \quad (8)$$

A discussion of the relation between K_p and $\Delta_r G^\circ$ in equation (7) can be found in various thermodynamics texts (e.g., Appendix I in Lewis 2004). Note that P_i is sometimes divided by the standard-state pressure of $P^\circ = 1$ bar, so that K_P remains a dimensionless quantity for reactions that have different numbers of products and reactants. The partial pressure of each constituent is a function of its mole fraction abundance X_i and the total pressure P_T ,

$$P_i = X_i P_T = \frac{[i]}{n} P_T. \quad (9)$$

The total number density of the system is calculated for a given volume from the ideal gas law,

$$n = \frac{P_T V N_A}{RT} = \frac{P_T}{k_B T}, \quad (10)$$

in which N_A is Avagadro's number and k_B is Boltzmann's constant (R/N_A). Substituting and rewriting equation (7) in units of number densities from equation (9) gives

$$K_P = \frac{[\text{C}]^c [\text{D}]^d}{[\text{A}]^a [\text{B}]^b} \left(\frac{P_T}{n} \right)^{(c+d-a-b)} = K_{eq} \left(\frac{P_T}{n} \right)^{(c+d-a-b)}, \quad (11)$$

where P_T is units of bars and $[i]$ and n are in units of molecules cm^{-3} . Rearrangement of this expression and substitution from equations (6) and (10) yields a general equation for calculating the reverse rate coefficient from the forward rate coefficient:

$$k_r = \frac{k_f}{e^{-\Delta_r G^\circ / RT}} (1.38065 \times 10^{-22} T)^{(n_p - n_r)}, \quad (12)$$

for T in kelvins, and where n_p and n_r are the numbers of products and reactants, respectively, in the forward reaction. Note that in cases where the number of products equals the number of reactants (*i.e.*, when $n_p - n_r = 0$), the pressure-correction term becomes unity and $K_P = K_{eq} = k_f/k_r$, as in equation (6).

For three-body (termolecular) reactions, the forward rate coefficient k_f used in equation (12) can be obtained from experimental or theoretical data at appropriate temperatures and pressures, and k_r can then be determined from the above procedure at each temperature-pressure point along the atmospheric grid. If k_f has not been measured at each P - T point along the grid, as is often the case, approximate expressions can be used. For example, the

rate coefficient at the low-pressure limit (k_0 in units of $\text{cm}^6 \text{s}^{-1}$) and high-pressure limit (k_∞ in units of $\text{cm}^3 \text{s}^{-1}$) have often been determined at a function of temperature. At intermediate pressures, k_f can be calculated from the expression

$$k_f = \frac{k_0}{1 + (k_0[\text{M}]/k_\infty)} F_c^\beta, \quad (13)$$

where β is given by

$$\beta = \left(1 + \left[\frac{\log_{10}(k_0[\text{M}]/k_\infty)}{0.75 - 1.27 \log_{10} F_c} \right]^2 \right)^{-1}, \quad (14)$$

and F_c is the center broadening factor (e.g., see Baulch et al. 2005).

As in our previous studies (Visscher et al. 2010; Moses et al. 2010), we calculate k_f for every pressure and temperature along the atmospheric grid, and then use equation (12) to determine k_r for the reverse of every reaction at each atmospheric level using the appropriate temperature- and pressure-dependent values for k_f and $\Delta_r G^\circ$. The outcome of this approach is a rate coefficient list of ~ 800 forward reactions and ~ 800 corresponding reverse reactions involving H-C-N-O species, for each atmospheric profile. As a result — when not including photochemistry and atmospheric transport, and given enough time to achieve steady state — our fully-reversed kinetics model yields results indistinguishable from those given by thermochemical-equilibrium calculations. Further description of the model can be found in Visscher et al. (2010) and Moses et al. (2010, 2011).

3. Model Results

3.1. CO Quench Chemistry on Gliese 229b

Results from our kinetics and transport model for Gliese 229B are given in Figure 2, which shows the CO abundance profiles for a $0.5\times$ protosolar-composition gas ($[\text{Fe}/\text{H}] = -0.3$) and various assumptions about the strength of vertical mixing (characterized by K_{zz} values from 10^3 to $10^9 \text{ cm}^2 \text{ s}^{-1}$). The dashed line indicates the thermochemical equilibrium mole fraction abundance of CO calculated along the atmospheric profile using the NASA CEA code (Gordon & McBride 1994). Also shown are determinations of the CO mole fraction from ground-based $4.7 \mu\text{m}$ observations of Gliese 229B (e.g., Noll et al. 1997; Oppenheimer et al. 1998; Griffith & Yelle 1999; Saumon et al. 2000). As predicted by Fegley & Lodders (1996), the observed CO abundance is several orders of magnitude larger than its equilibrium abundance in the observable regions of the atmosphere (see Figure 2), suggesting that CO is mixed upward from deeper regions where it is more favored thermodynamically.

In the deep atmosphere of Gliese 229B ($P_T \gtrsim 50$ bar), CO is the dominant carbon-bearing gas (cf. Figure 1), and its equilibrium abundance is maintained because the energy barriers for kinetic reactions are readily overcome at high temperatures. At lower pressures, CH₄ replaces CO as the dominant carbon-bearing gas under equilibrium conditions, and the equilibrium CO mole fraction rapidly decreases with altitude. However, at these colder altitudes, chemical reactions become more sluggish, and departures from equilibrium occur as atmospheric transport begins to dominate over reaction kinetics, eventually quenching the conversion of CO to CH₄. As shown in Figure 2, the depth of the quench level (and consequently, the quenched CO abundance) depends upon strength of vertical mixing: for stronger mixing (characterized by larger K_{zz} values) CO is quenched at relatively high pressures, deep in the atmosphere where it is more abundant; for weaker mixing (characterized by smaller K_{zz} values), CO is quenched at lower pressures and higher altitudes where it is less abundant at equilibrium. Above the quench level, CO is mixed upward at a constant mole fraction until it starts rapidly decreasing where molecular diffusion begins to dominate over eddy diffusion. In this scenario, the atmosphere no longer remains well mixed, and heavy species like CO become confined to lower altitudes. For very low K_{zz} values (e.g., $10^3 \text{ cm}^2 \text{ s}^{-1}$), the CO mole fraction does not remain constant above the quench level in our kinetics and transport model because molecular diffusion begins controlling atmospheric transport behavior at relatively high pressures.

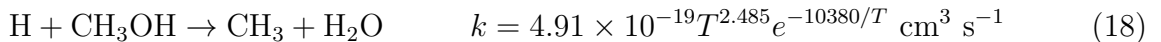
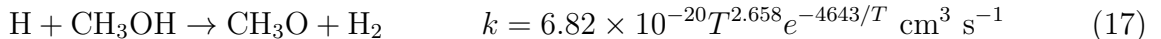
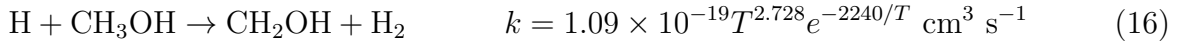
As noted in Visscher et al. (2010) and Moses et al. (2011), we identify the main chemical pathways from the model results by comparing the relative rates of all reactions in the model. Our results suggest that the dominant kinetic mechanism for CO \rightarrow CH₄ conversion in the troposphere of Gliese 229B consists of the following series of reactions:



where M represents any third body.

The slowest reaction in the fastest overall mechanism represents the rate-limiting step for CO \rightarrow CH₄ conversion on Gliese 229B. However, as discussed in Visscher et al. (2010),

there is a considerable degree of uncertainty in the identification of the rate-limiting step and the efficacy of the overall scheme, mostly due to uncertainties in laboratory and theoretical investigations of the product branching ratios for $\text{H} + \text{CH}_3\text{OH} \rightarrow \text{products}$ (see Visscher et al. 2010 for details) and for $\text{CH}_3 + \text{OH} \rightarrow \text{products}$ (e.g., see Jasper et al. 2007). These uncertainties prompted Moses et al. (2011) to use transition-state theory to calculate rate coefficients for the main $\text{H} + \text{CH}_3\text{OH}$ reaction pathways:



Adopting updated reaction rate coefficients for $\text{H} + \text{CH}_3\text{OH} \rightarrow \text{products}$ from Moses et al. (2011) and for $\text{CH}_3 + \text{OH} \rightarrow \text{products}$ from Jasper et al. (2007), we find that the thermal decomposition of methanol,



is the slowest reaction and is therefore the rate-limiting step for $\text{CO} \rightarrow \text{CH}_4$ conversion in the above scheme (15). This reaction mechanism differs from that originally proposed by Prinn & Barshay (1977), as well as that proposed by Yung et al. (1988) and adopted by Bézard et al. (2002) for Jupiter and by Griffith & Yelle (1999) for Gliese 229B because the updated rate coefficients were not previously available. The above scheme (15) also differs from that proposed by Visscher et al. (2010) for $\text{CO} \rightarrow \text{CH}_4$ in Jupiter’s troposphere, mostly due to differences in our selected reaction rate coefficients for $\text{H} + \text{CH}_3\text{OH} \rightarrow \text{CH}_3 + \text{H}_2\text{O}$ (Moses et al. 2011) and $\text{CH}_3 + \text{OH} \xrightarrow{\text{M}} \text{CH}_3\text{OH}$ (Jasper et al. 2007). Indeed, if we adopt the updated rate coefficients for our Jupiter models, the reaction scheme for CO destruction in Jupiter’s troposphere is identical to the scheme (15) described above for Gliese 229B. These revisions will also have some implications regarding the Jovian deep water abundance inferred from CO chemistry, which we briefly discuss in §3.3 below.

In any case, the rate-limiting reaction candidates identified in Visscher et al. (2010) all quench in the same vicinity in the atmosphere of Gliese 229B and are therefore expected to yield roughly similar results for the quench CO abundance if our adopted rate coefficients for any of the reactions in scheme (15) are in serious error. Furthermore, we emphasize that reaction (15e) is much more likely to be the rate-limiting step than the reaction $\text{H}_2 + \text{H}_2\text{CO} \rightarrow \text{CH}_3 + \text{OH}$ proposed by Prinn & Barshay (1977), which is too slow to play any significant role in CO quenching kinetics (e.g., Dean & Westmoreland 1987; Yung et al. 1988; De Avillez Pereira et al. 1997; Xia et al. 2001; Krasnoperov & Michael 2004; Baulch et al. 2005; Jasper et al. 2007) because there are faster, alternative pathways (such as scheme 15) for CO destruction in hydrogen-dominated substellar atmospheres.

Although the overall reaction scheme and/or the rate-limiting reaction for $\text{CO} \rightarrow \text{CH}_4$ conversion may differ for objects with different compositions or thermal profiles, we expect the above scheme to play an important role in the atmospheres of relatively cool (*i.e.*, $X_{\text{CH}_4} \approx X_{\Sigma\text{C}}$) substellar objects (such as T dwarfs or cool giant planets) with near-solar metallicities and element abundance ratios (e.g., \sim solar C/O). However, under some conditions the CO quenching mechanism may bypass CH_3OH altogether via the following mechanism:



in which the breaking of the C–O bond and the production of $\text{CH}_3 + \text{OH}$ is again the rate-limiting step, in this case via the reaction



Note that the *faster* of the two reactions (15e) or (19d) will serve as the rate-limiting step because this represents the fastest overall pathway available in our model for the $\text{CO} \rightarrow \text{CH}_4$ conversion process. However, although the thermal decomposition of methanol (reaction 15e) remains the dominant rate-limiting reaction over the range of K_{zz} values ($10^3 - 10^9 \text{ cm}^2 \text{ s}^{-1}$) shown in Figure 2, the contribution from reaction (19d) is significant enough (*i.e.*, it is fast enough) that it must be considered when estimating the quench CO abundance via a timescale approach.

Using the kinetic schemes identified above, we revisit the time-scale approach that was previously developed (e.g., Prinn & Barshay 1977; Fegley & Prinn 1985, 1988; Fegley & Lodders 1996; Lodders & Fegley 2002) to estimate the quenched abundance of CO in the atmosphere of cool giant planets and brown dwarfs. Considering reactions (15e) and (19d) as a combined rate-limiting step for CO destruction, the chemical lifetime of CO is given by

$$\tau_{chem}(\text{CO}) = \frac{[\text{CO}]}{-d[\text{CO}]/dt} \quad (20)$$

$$= \frac{[\text{CO}]}{k_{15e}[\text{M}][\text{CH}_3\text{OH}] + k_{19d}[\text{H}][\text{CH}_2\text{OH}]} \quad (21)$$

This expression is useful for considering the dominant contribution from either pathway breaking the C–O bond and forming $\text{CH}_3 + \text{OH}$. For example, if reaction (15e) is much faster than reaction (19d), $\tau_{chem}(\text{CO})$ will be mostly determined by the rate of the methanol decomposition reaction. The reaction rate coefficients k_{15e} and k_{19d} are calculated at each temperature in the model from their respective “forward” rate coefficients for $\text{CH}_3\text{OH} \xrightarrow{\text{M}} \text{CH}_3 + \text{OH}$ and $\text{H} + \text{CH}_2\text{OH} \rightarrow \text{CH}_3 + \text{OH}$ from Jasper et al. (2007), using equation (12) in the reversal procedure described above. The parameters used for calculating the forward rate coefficients are given below in our discussion of CH_4 quench chemistry on HD 189733b.

The vertical mixing time scale is given by

$$\tau_{mix} = \frac{L^2}{K_{zz}}, \quad (22)$$

where K_{zz} is the eddy diffusion coefficient and L is the characteristic length scale over which the mixing operates. Although the atmospheric pressure scale height H has commonly been used for L in time-scale comparisons, Smith (1998) has demonstrated that $L \approx H$ is not appropriate and that the mixing length L is some fraction of H that depends upon the thermal and eddy profiles of the substellar object, and upon the abundance profile of the atmospheric constituent (e.g., CO) under consideration. Using the procedure outlined in Smith (1998), Bézard et al. (2002) and Visscher et al. (2010) have confirmed that $L \sim 0.1H$ for CO quenching kinetics in Jupiter’s troposphere, and we find that $L \sim 0.1H$ to $0.3H$ is appropriate for CO quenching kinetics on Gliese 229B. A summary of results from our time-scale approach is given in Table 1, which lists L/H ratios for CO quenching for different values of K_{zz} .

The use of $L \approx H$ in chemical models involving $\text{CO} \rightleftharpoons \text{CH}_4$ quenching kinetics (along with the use of incorrectly calculated reverse rate coefficients; see §2.2) may have serious implications for vertical mixing estimates on brown dwarfs such as Gliese 229B, for which CO quench chemistry has been used to estimate the value of K_{zz} (Griffith & Yelle 1999). For example, earlier investigators have constrained K_{zz} on Gliese 229B to be in the range of $\sim 10^2 - 10^4 \text{ cm}^2 \text{ s}^{-1}$ based upon previous suggestions of the rate-limiting step and assuming $L \approx H$ (e.g., Griffith & Yelle 1999; Saumon et al. 2000; Leggett et al. 2007; Mainzer et al. 2007). One explanation for relatively low K_{zz} values is that the CO quench level could be in the radiative zone where convection no longer dominates, such that K_{zz} could approach the sluggish values typically found in planetary lower stratospheres (e.g., Griffith & Yelle 1999; Saumon et al. 2000, 2003). However, the predicted negative temperature gradient (Saumon et al. 2000) at the CO quench point of a few tens of bars on Gliese 229B is larger than is typically found in stagnant, low-mixing regions in planetary atmospheres (in fact, temperature gradients are typically positive in such stagnant regions where K_{zz} is inferred to be in the $\sim 10^2 - 10^4 \text{ cm}^2 \text{ s}^{-1}$ range in planetary atmospheres; see Yung & DeMore 1999). The

low derived K_{zz} values in the ~ 10 – 100 -bar region of Gliese 229B and other brown dwarfs are therefore surprising. However, in contrast to previous investigations, our thermochemical kinetics and transport model and model-data comparisons shown in Figure 2 suggest that the atmosphere of Gliese 229B is unlikely to be stagnant at the CO quench point. We find that K_{zz} values greater than $10^7 \text{ cm}^2 \text{ s}^{-1}$ are needed to explain the observed CO mole fraction of 60–600 ppm for assumed metallicities that range from $[\text{Fe}/\text{H}] = -0.5$ to -0.1 (Saumon et al. 2000, from an analysis of the $4.7 \mu\text{m}$ data of Noll et al. 1997 and Oppenheimer et al. 1998), or K_{zz} values greater $10^4 \text{ cm}^2 \text{ s}^{-1}$ are needed for the observed lower limit on the CO mole fraction of 20 ppm, for an assumed metallicity of $[\text{Fe}/\text{H}] = -0.6$ (Griffith & Yelle 1999). In comparison, free-convection and mixing-length theories (Stone 1976) predict a K_{zz} values of 10^8 to $10^9 \text{ cm}^2 \text{ s}^{-1}$ in the convection region of Gliese 229B. Our results therefore do not preclude strong convective mixing at the CO quench point on brown dwarfs like Gliese 229B.

We emphasize that the inferences with regard to the CO abundance on brown dwarfs remain the same with our updated time-constant procedure. It is simply the inferences with respect to K_{zz} that have changed. However, because assumptions about the strength of atmospheric mixing can affect cloud models and other theoretical predictions of the vertical transport of condensates and gas-phase species (e.g., Golimowski et al. 2004; Saumon et al. 2006, 2007; Leggett et al. 2007; Stephens et al. 2009; Spiegel et al. 2009), this change has important implications. When our rate-limiting step for CO quenching is considered and the Smith (1998) effective length scale is adopted, the CO-based evidence for sluggish mixing in the ~ 10 – 100 -bar region of Gliese 229B (and potentially other brown dwarfs) disappears.

The quench level for CO is defined as the altitude for which $\tau_{chem}(\text{CO}) = \tau_{mix}$. In the time-scale approach, the quenched CO mole fraction that is mixed to higher altitudes is equal to the equilibrium abundance achieved at the quench level (characterized by a temperature T_q and pressure P_q). The results from our updated time-scale approach for CO quenching kinetics on Gliese 229B are also illustrated in Figure 2, where the filled circles with dotted lines indicate the quenched CO abundance for each value of K_{zz} . In each case, the abundance estimated from the time-scale approach shows good agreement with the results from the full thermochemical kinetics and diffusion model (see Table 1). We therefore conclude that the time-scale approach provides a simple yet accurate method to describe the quench behavior of CO in the atmospheres of T dwarfs such as Gliese 229B — provided that a reasonable rate limiting step and appropriate rate coefficient are used for calculating τ_{chem} , and that the vertical mixing length scale L advocated by Smith (1998) is used for calculating τ_{mix} . Note that because several plausible $\text{CO} \rightarrow \text{CH}_4$ rate-limiting reactions tend to quench in the same vicinity, quenching investigations using the approach of Smith (1998) to estimate L give results similar to what would be expected from our kinetics and diffusion models (e.g., Bézard et al. 2002; Cooper & Showman 2006; Saumon et al. 2006, 2007; Geballe et al. 2009).

For some brown dwarfs, these models (e.g., Saumon et al. 2006, 2007; Geballe et al. 2009) indicate more sluggish mixing (i.e., lower K_{zz} values) near the CO quench level than what our results suggest here for Gliese 229B.

3.2. CH₄ Quench Chemistry on HD 189733b

The updated time-scale arguments also seem to be appropriate for describing the quenching of methane on HD 189733b. Figure 3 shows some results from the thermochemical kinetics and diffusion modeling of Moses et al. (2011) for an assumed solar-metallicity gas and variable assumptions about the rate of vertical transport (characterized by K_{zz} values from 10^7 to 10^{11} cm² s⁻¹) along the dayside-average and terminator-average profiles of HD 189733b. Also shown are CH₄ upper limits from secondary eclipse observations (corresponding to our dayside-average models) made with the NICMOS instrument onboard the *Hubble Space Telescope* (*HST*; Swain et al. 2008, 2009; Madhusudhan & Seager 2009) and with the IRAC instrument from the *Spitzer Space Telescope* (Charbonneau et al. 2008; Madhusudhan & Seager 2009), as well as CH₄ abundance determinations during transit observations (corresponding to our terminator-average models) using *HST*/NICMOS (Swain et al. 2008; Madhusudhan & Seager 2009).

The dashed lines in Figure 3 indicate the predicted thermochemical-equilibrium abundance of CH₄, calculated using the NASA CEA code (Gordon & McBride 1994). Methane is the dominant carbon-bearing gas in the deep atmosphere of HD 189733b ($P_T \gtrsim 10$ bar), but its equilibrium abundance rapidly decreases with altitude as it is replaced by CO. At high temperatures, the CH₄ abundance from the kinetics and transport models follows thermochemical equilibrium because forward and reverse reactions are relatively rapid (compared to mixing time scales) at high temperatures. At lower temperatures, however, atmospheric transport begins to dominate over reaction kinetics, and the conversion of CH₄ to CO becomes quenched. Disequilibrium abundances of CH₄ are therefore expected to be mixed into the upper atmosphere of HD 189733b (see also Cooper & Showman 2006; Line et al. 2010; Moses et al. 2011). As with CO quenching on Jupiter (Visscher et al. 2010) and Gliese 229B (§3.1), the transition from equilibrium to a quenched regime is not abrupt but occurs over a range of altitudes roughly equal to one pressure scale height. However, as we show for the CH₄ ⇌ CO quenching cases, the assumption of a quench point where $\tau_{chem} = \tau_{mix}$ along the equilibrium profile (as in the time-scale approach) seems to provide a reasonable approximation of the quenched abundance.

Comparison of the kinetics-with-transport model results for different K_{zz} profiles in Figure 3 illustrates the effect of the vertical mixing rate on CH₄ quench chemistry: for stronger

convective mixing (characterized by larger K_{zz}), CH_4 is quenched deeper in the atmosphere where it is more abundant; for weaker convective mixing (characterized by smaller K_{zz}), CH_4 is quenched at higher altitudes where it is less abundant. For very large K_{zz} values (e.g., $10^{11} \text{ cm}^2 \text{ s}^{-1}$) methane will quench at deep altitudes where it is the dominant C-bearing gas and will therefore represent a major portion of the atmospheric carbon inventory. In general, methane upper limits from the secondary eclipse observations are consistent with lower K_{zz} values (i.e., $K_{zz} \lesssim 10^8 \text{ cm}^2 \text{ s}^{-1}$) whereas the transit detections of methane are consistent with higher values (i.e., $K_{zz} \gtrsim 10^8 \text{ cm}^2 \text{ s}^{-1}$). Both photochemical destruction of CH_4 and transport-induced quenching on the warmer dayside would result in reduced CH_4 mole fractions on the dayside than at the terminators (Moses et al. 2011). However, the magnitude of these effects in the Moses et al. (2011) models is inconsistent with the observed dayside-terminator differences, and one might also expect strong zonal winds to homogenize the CH_4 with longitude, leaving the observed differences unexplained. As such, we cannot currently constrain K_{zz} on HD 189733b.

As is discussed in more detail in Moses et al. (2011), CH_4 destruction in the deep atmosphere of HD 189733b occurs via the following series of reactions:



where M refers to any third body. This scheme is exactly the reverse of the $\text{CO} \rightarrow \text{CH}_4$ conversion scheme for CO quench kinetics in the atmosphere of Gliese 229B and Jupiter (see §3.1). Using the revised rate coefficients for $\text{OH} + \text{CH}_3$ reaction pathways from Jasper et al. (2007) and $\text{H} + \text{CH}_3\text{OH}$ reaction pathways from Moses et al. (2011), the rate-limiting step (i.e., the slowest reaction) for the above scheme on HD 189733b is the reaction



which is the reverse of the rate-limiting step for CO destruction in the CH_4 -dominated atmosphere of Gliese 229B and Jupiter (§3.1). The temperature-dependent rate-coefficient for reaction (23c) is calculated via equation (13) using the modified Troe parameters given

in Jasper et al. (2007):

$$k_0 = 1.932 \times 10^3 T^{-9.88} e^{-7544/T} + 5.109 \times 10^{-11} T^{-6.25} e^{-1433/T} \text{ cm}^6 \text{ s}^{-1}, \quad (24)$$

$$k_\infty = 1.031 \times 10^{-10} T^{-0.018} e^{16.74/T} \text{ cm}^3 \text{ s}^{-1}, \quad (25)$$

$$F_c = 0.1855 e^{-T/155.8} + 0.8145 e^{-T/1675} + e^{-4531/T}, \quad (26)$$

As in the reverse scheme, under some conditions the CH₄ quenching process may bypass CH₃OH (i.e., reactions 23c and 23d) altogether, via the following mechanism :



in which the slowest reaction is the formation of the C–O bond via the OH + CH₃ reaction,



The rate coefficient for reaction (27c) at each level in the model is calculated using equation (13) with modified Troe parameters from Jasper et al. (2007):

$$k_0 = 1.092 \times 10^{-14} T^{0.996} e^{-1606/T} \text{ cm}^3 \text{ s}^{-1}, \quad (28)$$

$$k_\infty = 5.864 \times 10^{-6} T^{5.009} e^{-949.4/T} \text{ s}^{-1}, \quad (29)$$

$$F_c = 0.8622 e^{-T/9321} + 0.1378 e^{-T/361.8} + e^{-3125/T}. \quad (30)$$

As noted in Moses et al. (2011), the dominance of either reaction (23c) or reaction (27c) as the rate-limiting step in the CH₄ → CO mechanism depends upon the prevailing pressure and temperature conditions (e.g., Jasper et al. 2007). The CH₃OH-forming pathway (scheme 23) tends to dominate at higher pressures and higher K_{zz} values ($\gtrsim 10^9 \text{ cm}^2 \text{ s}^{-1}$), whereas the alternative pathway (scheme 27) tends to dominate at lower pressures and lower K_{zz} values ($\lesssim 10^9 \text{ cm}^2 \text{ s}^{-1}$) on HD 189733b. However, over the range of K_{zz} values considered here, the relative rates of reactions (23c) and (27c) are similar enough that both reactions should be considered when estimating the methane quench abundance in hot-Jupiter atmospheres.

Line et al. (2010) were the first to examine CH₄ quench chemistry on HD 189733b by calculating $\tau_{chem}(\text{CO})$ for CO → CH₄ conversion via the reaction $\text{H} + \text{H}_2\text{CO} \xrightarrow{\text{M}} \text{CH}_3\text{O}$

(Yung et al. 1988) and adopting $L = H$ for calculation of the vertical mixing time scale τ_{mix} . Aside from the omission of the pressure correction term when reversing $\text{CH}_3\text{O} + \text{M}$ (see §2.2), the use of $\tau_{chem}(\text{CO})$ and the reaction rate for $\text{H} + \text{H}_2\text{CO} + \text{M}$ rather than its reverse is acceptable but not preferable for determining *methane* quench behavior via the time-scale approach (in which it assumed that $k_f[\text{H}][\text{H}_2\text{CO}][\text{M}] = k_r[\text{CH}_3\text{O}][\text{M}]$ until quenching occurs). In the context of applying the Yung et al. (1988) kinetic scheme to HD 189733b, it would be more appropriate to calculate $\tau_{chem}(\text{CH}_4)$ for the reverse reaction $\text{CH}_3\text{O} \xrightarrow{\text{M}} \text{H}_2\text{CO} + \text{H}$ because it is the characterization of CH_4 quenching that is the main objective. Nevertheless, we recommend the use of the $\text{OH} + \text{CH}_3$ reactions $\text{OH} + \text{CH}_3 \xrightarrow{\text{M}} \text{CH}_3\text{OH}$ (23c) and $\text{OH} + \text{CH}_3 \rightarrow \text{CH}_2\text{OH} + \text{H}$ (27c) instead of $\text{CH}_3\text{O} \xrightarrow{\text{M}} \text{H}_2\text{CO} + \text{H}$ as the rate-limiting step for methane destruction in hot-Jupiter atmospheres, based upon a comparison of available $\text{CH}_4 \rightarrow \text{CO}$ reaction pathways and recent updates to reaction kinetics (Moses et al. 2011).

Using the reaction schemes (23) and (27) described above, we can now test revisions to the time-scale approach for estimating the quenched CH_4 mole fraction in the atmosphere of HD 189733b. Considering both $\text{OH} + \text{CH}_3$ pathways forming the C–O bond as a combined rate-limiting step provides a good estimate of the chemical lifetime for CH_4 , given by

$$\tau_{chem}(\text{CH}_4) = \frac{[\text{CH}_4]}{-d[\text{CH}_4]/dt}, \quad (31)$$

$$= \frac{[\text{CH}_4]}{k_{23c}[\text{M}][\text{CH}_3][\text{OH}] + k_{27c}[\text{CH}_3][\text{OH}]}. \quad (32)$$

The vertical mixing time scale (τ_{mix}) is given by equation (22). Using the procedure of Smith (1998), we obtain $L \sim 0.4H$ to $0.6H$ for CH_4 quenching kinetics in the atmosphere of HD189733b, depending upon the adopted K_{zz} value (cf. Cooper & Showman 2006, for HD 209458b). A summary of results from our time-scale approach for $K_{zz} = 10^7 - 10^{10} \text{ cm}^2 \text{ s}^{-1}$ is given in Table 2, which shows L/H values for CH_4 quenching via for different K_{zz} values in the atmosphere of HD 189733b. Note that the time-scale arguments generally compare very well (to within $\sim 10\%$ of) with the results of the thermochemical kinetics and transport model. We therefore confirm the analytical approach of Prinn & Barshay (1977) and conclude that the time-scale approach provides a simple yet accurate way to describe CH_4 quench chemistry in hot-Jupiter atmospheres — again, provided that the chemical time scale τ_{chem} is calculated using the appropriate rate-limiting step (*i.e.*, reactions 23c and 27c) and that the mixing time scale τ_{mix} is calculated using the appropriate vertical mixing length L (Smith 1998). However, the time-scale approximation begins to break down at very high K_{zz} values (e.g., $10^{11} \text{ cm}^2 \text{ s}^{-1}$; see Fig. 3) in our HD 189733b models: although CO begins to depart from equilibrium once $\tau_{chem} > \tau_{dyn}$, the nearly isothermal behavior of the atmosphere in this region (cf. Fig. 1) gives $\tau_{chem} \sim \tau_{dyn}$ over a wide range of altitudes above the quench level, so that there is no clear transition between the equilibrium and

quench regimes. In these cases, a kinetics and diffusion modeling approach is preferable for estimating the quench CH_4 abundance that is mixed into the upper atmosphere.

3.3. Revised Estimate of Jupiter’s Deep Water Abundance

As noted above, our preferred scheme for $\text{CO} \rightarrow \text{CH}_4$ in Jupiter’s troposphere differs from that proposed in previous studies of $\text{CO} \rightleftharpoons \text{CH}_4$ quench kinetics (e.g. Prinn & Barshay 1977; Yung et al. 1988; Bézard et al. 2002; Cooper & Showman 2006; Visscher et al. 2010; Line et al. 2010; Madhusudhan & Seager 2011) because of updates to reaction kinetics. The rate limiting step for CO destruction is $\text{H}_2 + \text{CH}_3\text{O} \rightarrow \text{CH}_3\text{OH} + \text{H}$ in the nominal model of Visscher et al. (2010). Our current scheme (15) includes CH_2OH as an intermediate instead of CH_3O , and the formation of CH_3 (which rapidly reacts to form CH_4) via $\text{CH}_3\text{OH} \xrightarrow{\text{M}} \text{CH}_3 + \text{OH}$ (15e) instead of $\text{H} + \text{CH}_3\text{OH} \rightarrow \text{CH}_3 + \text{H}_2\text{O}$. As noted above, these differences from Visscher et al. (2010) are mostly due to revisions in our adopted reaction rate coefficients for $\text{H} + \text{CH}_3\text{OH} \rightarrow \text{CH}_3 + \text{H}_2\text{O}$ (Moses et al. 2011) and $\text{CH}_3 + \text{OH} \xrightarrow{\text{M}} \text{CH}_3\text{OH}$ (Jasper et al. 2007), yielding a slower overall mechanism for $\text{CO} \rightarrow \text{CH}_4$ on Jupiter. Because CO quenching occurs at significantly higher pressures on Jupiter than on Gliese 229B, the reaction $\text{CH}_3\text{OH} \xrightarrow{\text{M}} \text{CH}_3 + \text{OH}$ (15e) is the dominant rate-limiting step in Jupiter’s troposphere. For example, assuming $K_{zz} = 10^8 \text{ cm}^2 \text{ s}^{-1}$, reaction (15e) is nearly two orders of magnitude faster than reaction (19d) at the quench level. Estimates of the quench CO abundance on Jupiter via the timescale approach therefore need only to consider the methanol decomposition reaction (15e) as the rate-limiting step for calculating the CO chemical lifetime.

The mechanism and rate of CO destruction in Jupiter’s troposphere has implications for the water abundance in Jupiter’s interior, because the CO abundance is closely tied to the H_2O abundance via the net thermochemical reaction (e.g., Fegley & Prinn 1988):



Because our revised $\text{CO} \rightarrow \text{CH}_4$ scheme is slower than that adopted by Visscher et al. (2010), quenching occurs deeper in the troposphere where CO is more thermodynamically favored. We therefore derive a lower estimate of the H_2O abundance than in Visscher et al. (2010). Adopting a CO mole fraction of 1.0 ± 0.2 ppb (Bézard et al. 2002) as an observational constraint for the internal/tropospheric CO source and considering a range of K_{zz} values from 1×10^7 to $1 \times 10^9 \text{ cm}^2 \text{ s}^{-1}$, our updated model results yield a Jovian water abundance of 0.1-1.5 times the solar $\text{H}_2\text{O}/\text{H}_2$ ratio (9.61×10^{-4}). For comparison, the preferred model in Visscher et al. (2010) gives a water abundance of 0.4-3.4 times the solar $\text{H}_2\text{O}/\text{H}_2$ ratio, not including uncertainties in reaction kinetics. We derive the following empirical expression

from the results of our kinetics and diffusion models:

$$X_{\text{CO}} = 6.52 \times 10^{-13} K_{zz}^{0.443} E_{\text{H}_2\text{O}}, \quad (34)$$

which describes the relationship between the CO mole fraction (X_{CO}), the eddy diffusion coefficient (K_{zz}), and the water enrichment over the solar abundance ($E_{\text{H}_2\text{O}}$) in Jupiter’s atmosphere, when $\text{CH}_3\text{OH} \xrightarrow{\text{M}} \text{CH}_3 + \text{OH}$ (15e) is the rate-limiting step for CO destruction.

Our model results suggest that the subsolar water abundance ($0.51 \times$ solar) measured by the *Galileo* entry probe (Wong et al. 2004) is consistent with the observed CO abundance (Bézard et al. 2002), and preclude formation mechanisms that would result in large water abundances in Jupiter’s atmosphere (e.g., see Lodders 2004 and Visscher et al. 2010 for discussion). If we take the *Galileo* entry probe H_2O abundance ($0.51 \times$ solar) as a lower limit and consider a factor-of-5 uncertainty in reaction kinetics for the rate-limiting step (e.g., Baulch et al. 2005), our models are consistent with a Jovian water abundance of 0.51–2.6 times the solar abundance, corresponding to $\text{H}_2\text{O}/\text{H}_2 \approx (4.9 - 25) \times 10^{-4}$ in the deep atmosphere. As noted above and in Visscher et al. (2010), we emphasize that this estimate is subject to revision based upon advances in our understanding of $\text{CO} \rightarrow \text{CH}_4$ reaction kinetics, as well as improvements in the determination of K_{zz} in Jupiter’s troposphere. Nevertheless, the plausible rate-limiting reactions for CO destruction generally imply lower water abundances than have been predicted from giant planet formation scenarios (e.g., Owen et al. 1999; Owen & Encrenaz 2006; Gautier et al. 2001; Hersant et al. 2004; Alibert et al. 2005; Mousis et al. 2009).

4. Conclusions

Our thermochemical kinetics and diffusion models for Gliese 229B and HD 189733b (see also Moses et al. 2011) confirm that atmospheric transport strongly influences the chemical behavior of carbon-bearing species in the upper atmospheres of substellar objects. Carbon monoxide is subject to transport-induced quenching on cool giant planets such as Jupiter and T dwarfs such as Gliese 229B, whereas methane may quench in the atmospheres of hot Jupiters such as HD 189733b. From a comparison of the relative rates of all available chemical pathways for $\text{CO} \rightleftharpoons \text{CH}_4$ interconversion in the thermochemical kinetics and transport models presented here and elsewhere (Visscher et al. 2010; Moses et al. 2011), we find that the destruction of the C–O bond is the rate-limiting step for CO quenching in the CH_4 -dominated objects, whereas formation of the C–O bond is the rate-limiting step for CH_4 quenching in the CO-dominated objects. Using updated reaction kinetics (Jasper et al. 2007; Moses et al. 2011) the dominant forward/reverse reaction pair for the formation/destruction of the C–O

bond is either $\text{OH} + \text{CH}_3 + \text{M} \rightleftharpoons \text{CH}_3\text{OH} + \text{M}$ or $\text{OH} + \text{CH}_3 \rightleftharpoons \text{CH}_2\text{OH} + \text{H}$, depending upon local temperature and pressure conditions near the quench level. However, because of their similar rates, both reaction pathways should be considered together when calculating τ_{chem} for $\text{CO} \rightleftharpoons \text{CH}_4$ quenching in brown dwarf or hot-Jupiter atmospheres. This reaction mechanism differs from the forward/reverse reaction pair $\text{H}_2 + \text{CH}_3\text{O} \rightleftharpoons \text{CH}_3\text{OH} + \text{H}$ proposed by Visscher et al. (2010), the forward/reverse reaction pair $\text{H} + \text{H}_2\text{CO} + \text{M} \rightleftharpoons \text{CH}_3\text{O} + \text{M}$ adopted by Yung et al. (1988) and subsequent authors (e.g., Griffith & Yelle 1999; Bézard et al. 2002; Cooper & Showman 2006; Saumon et al. 2006; Hubeny & Burrows 2007; Line et al. 2010; Madhusudhan & Seager 2011), or the original suggestion of $\text{H}_2 + \text{H}_2\text{CO} \rightleftharpoons \text{CH}_3 + \text{OH}$ by Prinn & Barshay (1977) and subsequent authors (e.g., Fegley & Prinn 1985, 1988; Fegley & Lodders 1996; Lodders & Fegley 1994, 2002; Saumon et al. 2003; Visscher & Fegley 2005; Hubeny & Burrows 2007) because of recent updates in reaction rate coefficients. These revisions also have implications for estimates of the water abundance in Jupiter’s deep troposphere using the CO observational constraint. Using updated kinetics, our model results along with a lower limit provided by *Galileo* entry probe measurements suggest a water abundance of approximately 0.51-2.6 times the solar abundance, corresponding to $\text{H}_2\text{O}/\text{H}_2 \approx (4.9 - 25) \times 10^{-4}$ in Jupiter’s deep atmosphere. The transport-induced quenching behavior of CO therefore implies lower H_2O abundances than have been predicted from several giant planet formation scenarios (e.g., see Lodders 2004; Visscher et al. 2010).

For each substellar object, the rate of vertical transport (characterized by eddy diffusion coefficient K_{zz}) will strongly affect the quenched abundance of a given species: for higher K_{zz} values, quenching occurs at deeper, hotter altitudes, whereas for lower K_{zz} values, quenching occurs at higher, cooler altitudes. Moreover, the equilibrium abundance of any atmospheric constituent at its quench level depends upon the bulk composition and thermal profile of the atmosphere (*i.e.*, the prevailing conditions at the quench point). The detection and characterization of quench species may therefore provide constraints on the chemistry, structure, and mixing rates of substellar atmospheres (e.g., Fegley & Lodders 1996; Lodders & Fegley 2002). For Gliese 229B, our results suggest significantly higher K_{zz} rates near the CO quench level than have been previously inferred. For HD 189733b, the terminator CH_4 detection by Swain et al. (2008) and the corresponding analysis by Madhusudhan & Seager (2009) suggest high values of K_{zz} ($\gtrsim 10^8 \text{ cm}^2 \text{ s}^{-1}$) at the $\text{CO} \rightleftharpoons \text{CH}_4$ quench point, whereas CH_4 upper limits for the dayside atmosphere as observed during secondary eclipse (Charbonneau et al. 2008; Madhusudhan & Seager 2009; Swain et al. 2008, 2009) suggest lower values of K_{zz} ($\lesssim 10^8 \text{ cm}^2 \text{ s}^{-1}$). These differences imply that disequilibrium chemistry, local K_{zz} differences, or other processes are complicating the simple picture of uniform transport-induced quenching in highly irradiated hot-Jupiter atmospheres.

We have presented an update to the time-constant procedure developed by Prinn &

Barshay (1977) and confirm that their general analytical approach can be used to accurately describe the chemical behavior of quenched species. In other words, full thermochemical kinetics and transport models are not needed to predict the quenched abundances of disequilibrium species, particularly for the case of CO and CH₄ quenching, for which there is one specific quench point (see also Visscher et al. 2010; Moses et al. 2011). We find that the time-scale approach can be used for a wide range of substellar objects to estimate the expected mole fractions of any atmospheric constituents subject to transport-induced quenching, provided that 1) an appropriate dominant mechanism for chemical interconversion between constituents is selected, which may require a comparison of the relative rates of all chemical pathways contributing to the production and destruction of the species under consideration, 2) an appropriate rate-limiting reaction within that dominant mechanism is identified, and the rate coefficient for that reaction is determined through laboratory or theoretical investigations (or proper reversal, if required) in order to calculate τ_{chem} , and 3) an appropriate mixing length L is adopted, following the procedure of Smith (1998), for the calculation of τ_{mix} . Previous questionable assumptions or incorrect applications of the time-constant procedure may have led to underestimates of the strength of atmospheric mixing at the CO quench level on Gliese 229B and inaccurate determinations of the methane abundance on extrasolar giant planets. Note that although the time-constant approach is not limited to $\text{CO} \rightleftharpoons \text{CH}_4$ but can be applied to any chemical constituent subject to reaction kinetics and vertical mixing in substellar atmospheres (e.g., see the discussion of the quenching of nitrogen species on Jupiter by Moses et al. 2010), some constituents such as HCN or NH₃ may have complicated quench kinetics (Moses et al. 2011), making the time-constant arguments difficult to apply in practice. The time-scale approximation may also break down if $\tau_{chem} \sim \tau_{mix}$ over an extended pressure range, due to small temperature gradients (such as can be found in radiative regions) or other conditions. As such, thermochemical kinetics and transport models may still have an important role to play in the prediction of transport-quenched abundances in the atmospheres of substellar objects.

Acknowledgements

We thank Justin Troyer for contributing to preliminary kinetics and diffusion models of Gliese 229B. This work was supported by the NASA Planetary Atmospheres Program (NNH08ZDA001N). Support for C.V. was also provided by the Lunar and Planetary Institute, USRA (NASA Cooperative Agreement NCC5-679). LPI Contribution No. 1624.

REFERENCES

- Alibert, Y., Mousis, O., & Benz, W. 2005, *Astrophysical Journal Letters*, 622, L145
- Allen, M., Yung, Y. L., & Waters, J. W. 1981, *J. Geophys. Res.*, 86, 3617
- Barshay, S. S., & Lewis, J. S. 1978, *Icarus*, 33, 593
- Baulch, D. L. et al. 2005, *Journal of Physical and Chemical Reference Data*, 34, 757
- Bézard, B., Lellouch, E., Strobel, D., Maillard, J.-P., & Drossart, P. 2002, *Icarus*, 159, 95
- Burrows, A., Budaj, J., & Hubeny, I. 2008, *ApJ*, 678, 1436
- Charbonneau, D., Knutson, H. A., Barman, T., Allen, L. E., Mayor, M., Megeath, S. T., Queloz, D., & Udry, S. 2008, *ApJ*, 686, 1341
- Chase, M. W. 1998, *Journal of Physical and Chemical Reference Data*, 28, Monograph No. 9, New York: AIP
- Cooper, C. S., & Showman, A. P. 2006, *ApJ*, 649, 1048
- De Avillez Pereira, R., Baulch, D. L., Pilling, M. J., Robertson, S. H., & Zeng, G. 1997, *Journal of Physical Chemistry A*, 101, 9681
- Dean, A., & Westmoreland, P. 1987, *International Journal of Chemical Kinetics*, 19, 207
- Fegley, Jr., B., Gautier, D., Owen, T., & Prinn, R. G. 1991, in *Uranus*, ed. J. T. Bergstrahl, E. D. Miner, & M. S. Matthews (Tucson: Univ. of Arizona Press), 147–203
- Fegley, Jr., B., & Lewis, J. S. 1979, *Icarus*, 38, 166
- Fegley, Jr., B., & Lodders, K. 1994, *Icarus*, 110, 117
- . 1996, *Astrophysical Journal Letters*, 472, L37
- Fegley, Jr., B., & Prinn, R. G. 1985, *Astrophysical Journal*, 299, 1067
- . 1986, *Astrophysical Journal*, 307, 852
- . 1988, *Astrophysical Journal*, 324, 621
- Flasar, F. M., & Gierasch, P. J. 1977, in *Planetary Atmospheres*, ed. A. V. Jones, Proceedings of the Nineteenth Symposium of the Royal Society of Canada (Ottawa: Royal Society of Canada), 85

- Fortney, J. J., Cooper, C. S., Showman, A. P., Marley, M. S., & Freedman, R. S. 2006a, *ApJ*, 652, 746
- Fortney, J. J., Saumon, D., Marley, M. S., Lodders, K., & Freedman, R. S. 2006b, *Astrophysical Journal*, 642, 495
- Fouchet, T., Moses, J. I., & Conrath, B. J. 2009, in *Saturn from Cassini-Huygens*, ed. Dougherty, M. K., Esposito, L. W., & Krimigis, S. M. (Berlin: Springer), 83–112
- García Muñoz, A. 2007, *Planet. Space Sci.*, 55, 1426
- Gautier, D., Hersant, F., Mousis, O., & Lunine, J. I. 2001, *Astrophysical Journal Letters*, 550, L227 (erratum 559, L183)
- Geballe, T. R., Saumon, D., Golimowski, D. A., Leggett, S. K., Marley, M. S., & Noll, K. S. 2009, *ApJ*, 695, 844
- Golimowski, D. A. et al. 2004, *Astronomical Journal*, 127, 3516
- Gordon, S., & McBride, B. J. 1994, *NASA Reference Publication* 1311
- Griffith, C. 2000, in *Astronomical Society of the Pacific Conference Series*, Vol. 212, *From Giant Planets to Cool Stars*, ed. C. A. Griffith & M. S. Marley, 142–151
- Griffith, C. A., & Yelle, R. V. 1999, *Astrophysical Journal Letters*, 519, L85
- Griffith, C. A., Yelle, R. V., & Marley, M. S. 1998, *Science*, 282, 2063
- Hersant, F., Gautier, D., & Lunine, J. I. 2004, *Planetary and Space Science*, 52, 623
- Hubeny, I., & Burrows, A. 2007, *ApJ*, 669, 1248
- Jasper, A., Klippenstein, S., Harding, L., & Ruscic, B. 2007, *J. Phys. Chem. A*, 111, 3932
- King, R. R., McCaughrean, M. J., Homeier, D., Allard, F., Scholz, R., & Lodieu, N. 2010, *A&A*, 510, A99
- Krasnoperov, L., & Michael, J. 2004, *Journal of Physical Chemistry A*, 108, 8317
- Leggett, S. K., Saumon, D., Marley, M. S., Geballe, T. R., Golimowski, D. A., Stephens, D., & Fan, X. 2007, *ApJ*, 655, 1079
- Lewis, J. S. 2004, *Physics and Chemistry of the Solar System*, 2nd edn., *International Geophysics Series*, Volume 87 (Elsevier Academic Press)

- Lewis, J. S., & Fegley, Jr., M. B. 1984, *Space Science Reviews*, 39, 163
- Lewis, N. K., Showman, A. P., Fortney, J. J., Marley, M. S., Freedman, R. S., & Lodders, K. 2010, *ApJ*, 720, 344
- Liang, M.-C., Parkinson, C. D., Lee, A. Y.-T., Yung, Y. L., & Seager, S. 2003, *Astrophysical Journal Letters*, 596, L247
- Liang, M.-C., Seager, S., Parkinson, C. D., Lee, A. Y.-T., & Yung, Y. L. 2004, *Astrophysical Journal Letters*, 605, L61
- Line, M. R., Liang, M. C., & Yung, Y. L. 2010, *ApJ*, 717, 496
- Lodders, K. 2004, *Astrophysical Journal*, 611, 587
- Lodders, K., & Fegley, Jr., B. 1994, *Icarus*, 112, 368
- . 2002, *Icarus*, 155, 393
- Lodders, K., Palme, H., & Gail, H. 2009, *arXiv:0901.1149*
- Madhusudhan, N., & Seager, S. 2009, *ApJ*, 707, 24
- . 2011, *ApJ*, 729, 41
- Mainzer, A. K. et al. 2007, *ApJ*, 662, 1245
- Moses, J. I. et al. 2011, *ApJ*, in press, *arXiv:1102.0063*
- Moses, J. I., Visscher, C., Keane, T. C., & Sperier, A. 2010, *Faraday Discussions*, 147, 103
- Mousis, O., Marboeuf, U., Lunine, J. I., Alibert, Y., Fletcher, L. N., Orton, G. S., Pauzat, F., & Ellinger, Y. 2009, *ApJ*, 696, 1348
- Noll, K. S., Geballe, T. R., & Marley, M. S. 1997, *ApJ*, 489, L87
- Oppenheimer, B. R., Kulkarni, S. R., Matthews, K., & van Kerkwijk, M. H. 1998, *ApJ*, 502, 932
- Owen, T., & Encrenaz, T. 2006, *Planet. Space Sci.*, 54, 1188
- Owen, T., Mahaffy, P., Niemann, H. B., Atreya, S., Donahue, T., Bar-Nun, A., & de Pater, I. 1999, *Nature*, 402, 269
- Page, M., Lin, M. C., He, Y., & Choudhury, T. K. 1989, *J. Phys. Chem.*, 93, 4404

- Prinn, R. G., & Barshay, S. S. 1977, *Science*, 198, 1031
- Prinn, R. G., Larson, H. P., Caldwell, J. J., & Gautier, D. 1984, in *Saturn*, ed. T. Gehrels & M. S. Matthews (Tucson: Univ. of Arizona Press), 88–149
- Prinn, R. G., & Olaguer, E. P. 1981, *Journal of Geophysical Research*, 86, 9895
- Prinn, R. G., & Owen, T. 1976, in *Jupiter*, ed. T. Gehrels (Tucson: Univ. of Arizona Press), 319–371
- Saumon, D., Geballe, T. R., Leggett, S. K., Marley, M. S., Freedman, R. S., Lodders, K., Fegley, B., & Sengupta, S. K. 2000, *Astrophysical Journal*, 541, 374
- Saumon, D., Marley, M. S., Cushing, M. C., Leggett, S. K., Roellig, T. L., Lodders, K., & Freedman, R. S. 2006, *ApJ*, 647, 552
- Saumon, D. et al. 2007, *ApJ*, 656, 1136
- Saumon, D., Marley, M. S., Lodders, K., & Freedman, R. S. 2003, in *IAU Symposium*, Vol. 211, *Brown Dwarfs*, ed. E. Martín, 345
- Showman, A. P., Fortney, J. J., Lian, Y., Marley, M. S., Freedman, R. S., Knutson, H. A., & Charbonneau, D. 2009, *ApJ*, 699, 564
- Smith, M. D. 1998, *Icarus*, 132, 176
- Spiegel, D. S., Silverio, K., & Burrows, A. 2009, *ApJ*, 699, 1487
- Stephens, D. C. et al. 2009, *ApJ*, 702, 154
- Stevenson, K. B. et al. 2010, *Nature*, 464, 1161
- Stone, P. H. 1976, in *Jupiter*, ed. T. Gehrels (Tucson: Univ. of Arizona Press), 586–618
- Swain, M. R. et al. 2009, *ApJ*, 704, 1616
- Swain, M. R., Vasisht, G., & Tinetti, G. 2008, *Nature*, 452, 329
- Taylor, F. W., Atreya, S. K., Encrenaz, T., Hunten, D. M., Irwin, P. G. J., & Owen, T. C. 2004, in *Jupiter. The Planet, Satellites and Magnetosphere*, ed. F. Bagenal, T. E. Dowling, & W. B. McKinnon (Cambridge: Cambridge Univ. Press), 59–78
- Visscher, C., & Fegley, Jr., B. 2005, *Astrophysical Journal*, 623, 1221
- Visscher, C., Lodders, K., & Fegley, Jr., B. 2006, *Astrophysical Journal*, 648, 1181

- Visscher, C., Moses, J. I., & Saslow, S. A. 2010, *Icarus*, 209, 602
- Wong, M. H., Mahaffy, P. R., Atreya, S. K., Niemann, H. B., & Owen, T. C. 2004, *Icarus*, 171, 153
- Xia, W. S., Zhu, R. S., Lin, M. C., & Mebel, A. M. 2001, *Faraday Discussions*, 119, 191
- Yamamura, I., Tsuji, T., & Tanabé, T. 2010, *ApJ*, 722, 682
- Youdin, A. N., & Mitchell, J. L. 2010, *ApJ*, 721, 1113
- Yung, Y. L., & DeMore, W. B. 1999, *Photochemistry of Planetary Atmospheres* (New York: Oxford Univ. Press)
- Yung, Y. L., Drew, W. A., Pinto, J. P., & Friedl, R. R. 1988, *Icarus*, 73, 516
- Zahnle, K., Marley, M. S., & Fortney, J. J. 2009a, *ApJ*, submitted, arXiv:astro-ph/0911.0728
- Zahnle, K., Marley, M. S., Freedman, R. S., Lodders, K., & Fortney, J. J. 2009b, *ApJ*, 701, L20

Table 1. CO quench chemistry on Gliese 229B

K_{zz} , $\text{cm}^2 \text{s}^{-1}$	time-scale approach					kinetics model
	T_q , K	P_q , bar	$\tau_{chem}(\text{CO})$, s	L/H	quenched X_{CO}	quenched X_{CO}
1×10^3	1295	10.4	4.16×10^6	0.140	1.69×10^{-5}	1.33×10^{-5}
1×10^5	1457	17.8	8.71×10^4	0.181	4.70×10^{-5}	4.09×10^{-5}
1×10^7	1651	33.2	1.82×10^3	0.230	8.53×10^{-5}	7.83×10^{-5}
1×10^9	1910	64.9	3.29×10^1	0.268	1.26×10^{-4}	1.19×10^{-4}

Note. — For the kinetics models, the CO mole fraction at the 1-bar level is adopted as the quenched abundance.

Table 2. CH_4 quench chemistry on HD 189733b

K_{zz} , $\text{cm}^2 \text{s}^{-1}$	time-scale approach					kinetics model
	T_q , K	P_q , bar	$\tau_{chem}(\text{CH}_4)$, s	L/H	quenched X_{CH_4}	quenched X_{CH_4}
dayside-average thermal-structure models						
1×10^7	1394	0.5	7.86×10^6	0.383	2.92×10^{-6}	3.11×10^{-6}
1×10^8	1455	0.8	1.09×10^6	0.435	4.37×10^{-6}	4.66×10^{-6}
1×10^9	1516	1.8	1.67×10^5	0.518	8.89×10^{-6}	9.64×10^{-6}
1×10^{10}	1573	5.8	2.62×10^4	0.630	4.18×10^{-5}	4.05×10^{-5}
terminator-average thermal-structure models						
1×10^7	1389	1.1	6.70×10^6	0.359	1.60×10^{-5}	1.68×10^{-5}
1×10^8	1448	1.9	9.79×10^5	0.415	2.14×10^{-5}	2.27×10^{-5}
1×10^9	1506	3.6	1.53×10^5	0.502	4.31×10^{-5}	4.25×10^{-5}
1×10^{10}	1548	11.0	3.12×10^4	0.702	1.28×10^{-4}	1.20×10^{-4}

Note. — For the kinetics models, the CH_4 mole fraction at the 0.01-bar level is adopted as the quenched abundance.

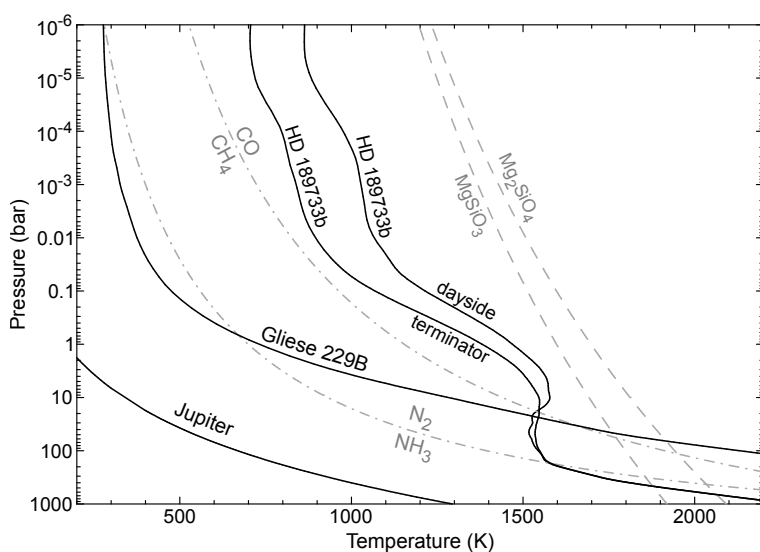


Fig. 1.— Pressure-temperature profiles (solid lines) used in our models for Gliese 229B, based upon Model B in Saumon et al. (2000) and dayside-average and terminator-average profiles for HD 189733b from Moses et al. (2011), based upon the GCM results of Showman et al. (2009). The atmospheric profile for Jupiter is shown for comparison. Also shown are thermochemical equilibrium equal-abundance boundaries (dash-dotted lines) for major nitrogen (NH_3 , N_2) and carbon (CH_4 , CO) gases and the equilibrium condensation curves (dashed lines) for forsterite (Mg_2SiO_4) and enstatite (MgSiO_3) in a solar-metallicity gas (Lodders et al. 2009).

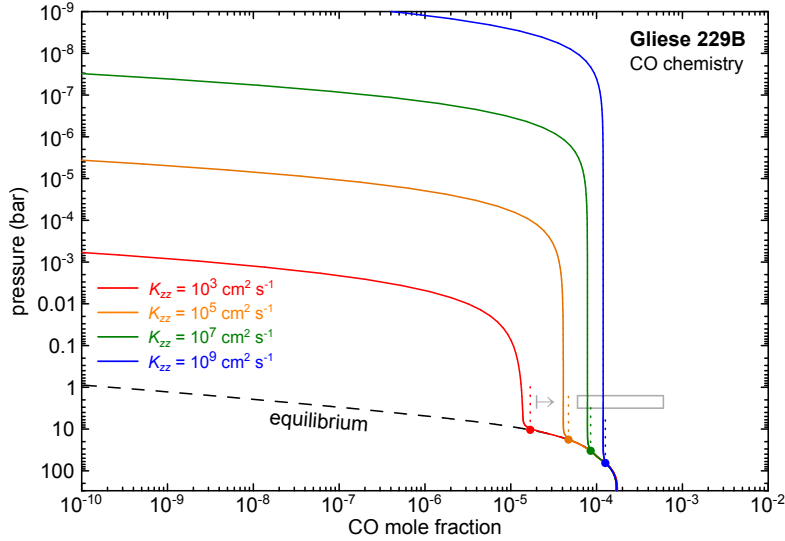


Fig. 2.— CO chemistry in the atmosphere of Gliese 229B for models considering thermochemical equilibrium only (dashed line) and thermochemistry with transport (solid lines) assuming K_{zz} values of 10^3 , 10^5 , 10^7 , and 10^9 $\text{cm}^2 \text{s}^{-1}$ and a $0.5\times$ protosolar ($[\text{Fe}/\text{H}] = -0.3$) composition (Saumon et al. 2000; Lodders et al. 2009). For each case, the drop in the in the CO abundance at very low pressures illustrates where molecular diffusion begins to dominate over eddy diffusion. The gray box shows a CO mole fraction of 60 – 600 ppm based upon the $4.7 \mu\text{m}$ observations of Noll et al. (1997) and Oppenheimer et al. (1998) for metallicities ranging from $[\text{Fe}/\text{H}] = -0.5$ to -0.1 in the models of Saumon et al. (2000). The vertical gray bar with arrow represents a lower limit to the CO abundance of $X_{\text{CO}} \geq 20$ ppm from an analysis of the Noll et al. (1997) data by Griffith & Yelle (1999), assuming a metallicity of $[\text{Fe}/\text{H}] \approx -0.6$. The filled circles with dotted lines show the quench level (where $\tau_{chem} = \tau_{mix}$) and quenched CO mole fraction, respectively, as derived from the updated time-scale approach for each value of K_{zz} .

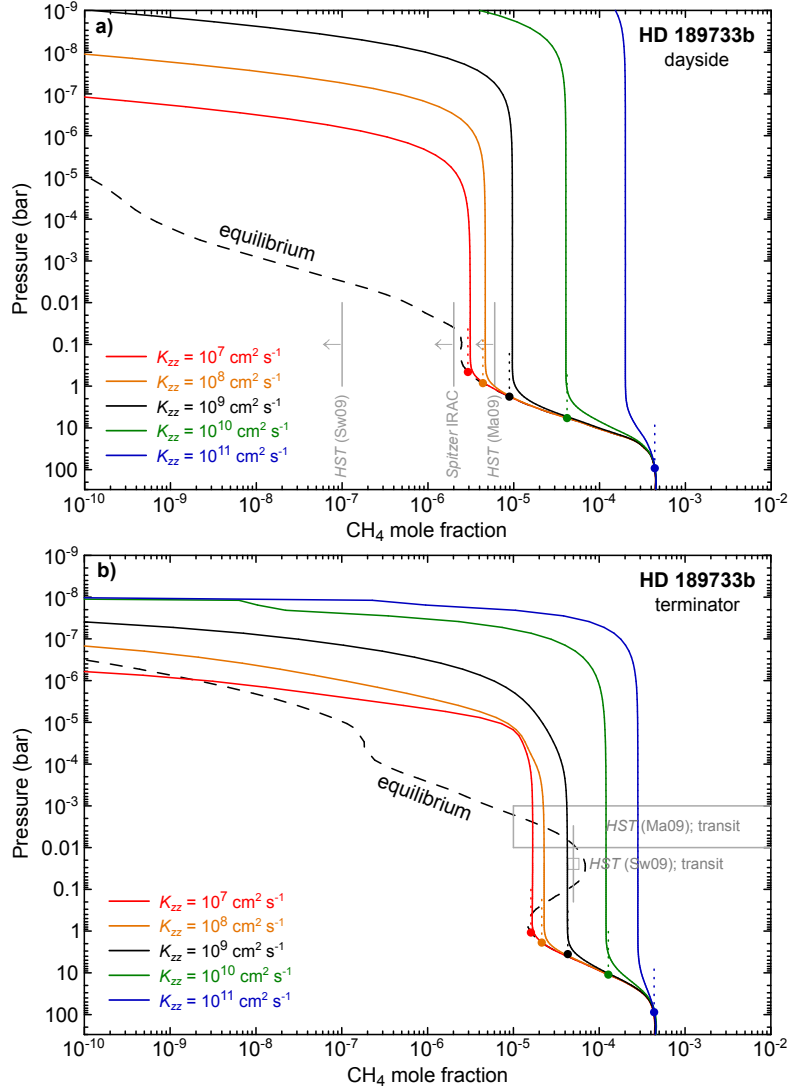


Fig. 3.— CH_4 chemistry in the atmosphere of HD 189733b (profiles from Moses et al. 2011) for a) dayside-average models and b) terminator-average models, considering thermochemical equilibrium only (dashed line) and thermochemistry with transport (solid lines) assuming solar-metallicity composition (Lodders et al. 2009) and a range of K_{zz} values (as labeled). For each case, the drop-off in the CH_4 abundance at very low pressures illustrates where molecular diffusion begins to dominate over eddy diffusion. In the dayside-average plot, the vertical gray bars with arrows represent upper limits on the methane abundance from *HST*/NICMOS (Swain et al. 2009; Madhusudhan & Seager 2009) and *Spitzer*/IRAC (Madhusudhan & Seager 2009; Charbonneau et al. 2008) observations for $0.01 < P_T < 1$ bar after Swain et al. (2009); upper limits from Madhusudhan & Seager (2009) are shown at similar pressures for comparison. In the terminator-average plot, detections of methane from *HST*/NICMOS transit observations are indicated by gray boxes. Swain et al. (2008) derive a best-fitting CH_4 mole fraction of 5×10^{-5} , whereas Madhusudhan & Seager (2009) find that CH_4/H_2 mixing ratios from 10^{-5} to 0.3 are consistent with the transmission spectra. The filled circles with dotted lines show the quench level (where $\tau_{chem} = \tau_{mix}$) and quenched CH_4 mole fraction, respectively, as derived from the time-scale approach for each value of K_{zz} .